

VLT Optical *BVR* observations of two bright Supernova Ia hosts in the Virgo cluster

Surface Brightness Fluctuations analysis

Michele Cantiello¹, Ilaria Biscardi^{1,2}, Enzo Brocato¹, and Gabriella Raimondo¹

¹ INAF-Osservatorio Astronomico di Teramo, via M. Maggini snc, I-64100, Teramo, Italy
e-mail: cantiello@oa-teramo.inaf.it

² Dipartimento di Fisica – Università di Roma Tor Vergata, via della Ricerca Scientifica 1, 00133 Rome, Italy

Received —; accepted —

ABSTRACT

Aims. We study the characteristics of field stars in the two bright ellipticals NGC 4621 and NGC 4374 in the Virgo cluster to derive distances and stellar population properties. Moreover, since the target galaxies have hosted three type Ia Supernova events, we investigate the correlations between the SNeIa properties and their host stellar systems.

Methods. Using deep imaging *BVR* data, obtained with the FORS2 camera mounted at the VLT, we analyse the Surface Brightness Fluctuations (SBF) properties of the targets. We adopt our measurements and existing empirical or theoretical calibrations to estimate the distance of the NGC 4621 and NGC 4374. For stellar population analysis, we measured SBF amplitudes in different galaxy regions, allowing to study the changes in field star properties. The three band coverage of present data, coupled with existing SBF measures available from literature, provides us with the largest wavelength coverage of SBF magnitudes for single objects. We present a detailed comparison between SBF data and models to constrain the physical characteristics of the dominant stellar components at *i*) various galactic radii, and *ii*) in the regions where SNeIa events were recorded.

Results. Our *V* and *R* SBF measures provide distances in agreement with literature estimates. The median of our and literature SBF-based distances agrees with the one from non-SBF methods, indicating the absence of any systematic effect in the SBF technique. Comparing either the SBF versus integrated colour diagrams, or the SBF versus SBF colour diagrams, with models, we find that stellar populations properties do not change significantly along galactic radius, with a dominant population having old age and solar chemical composition. The galaxies appear similar in all properties analysed, except for *B*-band SBF. Since the SBF magnitudes in this band are sensitive to the properties of the hot stellar component, we speculate that such behaviour is a consequence of different diffuse hot stellar components in the galaxies. Using specific models we find that the presence of a percentage of hot-HB stars in old and metal rich stellar populations could be at the origin of the observed differences. We find a good uniformity in the *V* and *R* SBF and integrated colours in the regions where the three SNeIa, presenting different absolute luminosities, exploded. On the other hand, the *B*-band SBF signal shows intriguing differences.

Key words. Galaxies: distances and redshifts – Galaxies: elliptical and lenticular, cD – Galaxies: stellar content – Galaxies: photometry – Galaxies: individual: NGC 4621, NGC 4374

1. Introduction

Our understanding of galaxies in the distant Universe relies on how well we understand the properties of their local templates. Thus, the study of nearby unresolved stellar populations plays a key role to obtain a refined characterisation of stellar populations at larger redshifts. Although different astronomical methods exist to carry out such detailed analysis, none of them can provide by itself robust constraints. The presence of internal uncertainties in each method, or calibration uncertainties, as well as the effect of the age-metallicity degeneracy that affects most of the spectro-photometric indicators (Worthey 1994), prevents us from relying on one single stellar population tracer for these studies, and pushes the community of astronomers towards the definition of new analysis methods.

In the last two decades, the SBF method, introduced by Tonry & Schneider (1988) to obtain distances of early-type

galaxies, has proved being not only an accurate and precise distance indicator, but also a powerful tracer of stellar population properties (e.g. Jensen et al. 2003; Raimondo et al. 2005; Cantiello et al. 2007b). By definition, the SBF magnitude corresponds to the ratio of the second to the first moment of the stellar luminosity function in the galaxy: $\bar{m} = -2.5 \log \bar{f}$, where $\bar{f} \equiv \frac{\sum_i n_i f_i^2}{\sum_i n_i f_i}$, and n_i is the number of stars per bin of flux f_i (Tonry & Schneider 1988). Such definition implies that: *(i)* SBF magnitudes are linked to the properties of the stars in the galaxy; *(ii)* the SBF signal is dominated by the brightest stellar component in the galaxy, because of the dependence on the second moment of the luminosity function; *(iii)* since the brightest phase in a stellar population is wavelength-dependent, SBF magnitudes in different pass-bands are sensitive to the properties of stars in different, and well defined, evolutionary stages (Worthey 1993a; Brocato et al. 1998; Cantiello et al. 2003).

Table 1. Main parameters of the target galaxies and observations

	NGC 4621	NGC 4374
Galaxy parameters		
RA(J2000) ¹	12h42m02.3s	12h25m03.7s
Dec(J2000) ¹	+11d38m49s	+12d53m13s
Galaxy Type ²	E5	E
Morphological Type ²	-4.8	-4.3
Absolute <i>B</i> -band magnitude ²	-20.5	-21.0
SNe Ia events	SN1939B	SN1957B, SN1991bg
<i>cz</i> ¹ (km/s, Heliocentric)	410±6	1060 ±6
<i>E(B-V)</i> ³	0.033 mag	0.040 mag
<i>(V-I)</i> ⁴	1.172 ± 0.018	1.191±0.008
Observations		
Filter	Exposure time (s)	Exposure time (s)
<i>B</i>	3375	2250
<i>V</i>	3375	2250
<i>R</i>	2376	1584

¹ Data retrieved from NED (<http://nedwww.ipac.caltech.edu>); ² Hyperleda (<http://leda.univ-lyon1.fr>); ³ Schlegel et al. (1998);

⁴ Tonry et al. (2001)

Taking advantage of archival *B*, *V*, and *R* observations taken with the FORS2 camera of the Very Large Telescope for two bright early-type galaxies in the Virgo cluster, NGC 4621 and NGC 4374, we obtain multi-band SBF measurements of these galaxies. These measurements, coupled with existing ground-based *I*– and *K*–band measures, and space-based *F850LP* from ACS data (*z* hereafter; for integrated colours we will also use ACS *F475W* data, indicated as *g* in the paper), provide the largest wavelength coverage of SBF measures for single galaxies. With such sample of measures we investigate the properties of the two galaxies using the SBF technique under its twofold aspects: as a distance indicator and as a stellar population properties tracer. Furthermore, since the target galaxies have hosted three SNe Ia events – SN 1939B in NGC 4621 (Zwicky 1942), and SN 1957B (Bertola 1964, and references therein) plus SN 1991bg (Kosai et al. 1991) in NGC 4374 – we can explore the capabilities of the SBF method to improve our knowledge on the relation between the SNe Ia progenitors and the stellar population they belong to.

The paper is organised as follows: a description of the observational data set, the data reduction and calibration procedures, and the procedure for SBF measurements is given in §2. The analysis of distances is presented in §3, while the study of stellar population properties based on SBF is presented in §4. A summary and the conclusions finish the paper in §5.

2. The Data

For this work we used *B*, *V* and *R* data of two Virgo cluster galaxies, NGC 4621 and NGC 4374, observed with the FORS2 camera of the VLT. Some relevant properties of the targets are reported in Table 1.

The science images of the galaxies and the calibration files (bias, flat, field of standard stars) were retrieved from the ESO archive¹.

In one case, NGC 4374, we could not use the total integration time available because of a slight rotation ($\lesssim 1$ deg)

between different frames which badly affects the SBF signal (see below). In Table 1 we list the total exposure times for each filter and for both galaxies.

2.1. Data reduction and calibration

All data were retrieved from the archive and processed with standard data reduction procedures using IRAF² tasks. The procedure is briefly described here. We obtained master bias and flat frames (one per filter) for each observing night. Individual frames are bias-subtracted, flattened, shifted into registration, and combined, rejecting pixels affected by cosmic ray hits. To combine the frames we imposed no sub-pixel registration, in order to avoid the contamination to SBF due to the sub-pixel interpolation (Jensen et al. 1998). Finally, the seeing between targets and filters ranged between 0".8 and 1".0. The combined frames are shown in Figure 1.

The standard calibration plan of FORS2 provides nightly multi-band observations of Landolt (1992) standards, which are used to calibrate the photometry of the two galaxies.

2.2. Data analysis and SBF measurements

To derive the photometry of sources in the frames and measure the fluctuation amplitudes we used the same procedure described in our previous works (Cantiello et al. 2005, 2007a,b, 2009; Biscardi et al. 2008). The main steps of SBF measurement involve: sky background determination, model and large scale residual subtraction; photometry and masking of point-like and extended sources, including dust; power spectrum analysis of the residual frame.

Here we briefly describe some relevant parts of the analysis. We determined the sky background in the galaxy images by fitting the surface brightness profile of the galaxy

² IRAF is distributed by the National Optical Astronomy Observatories, which are operated by the Association of Universities for Research in Astronomy, Inc., under cooperative agreement with the National Science Foundation.

¹ <http://archive.eso.org/>

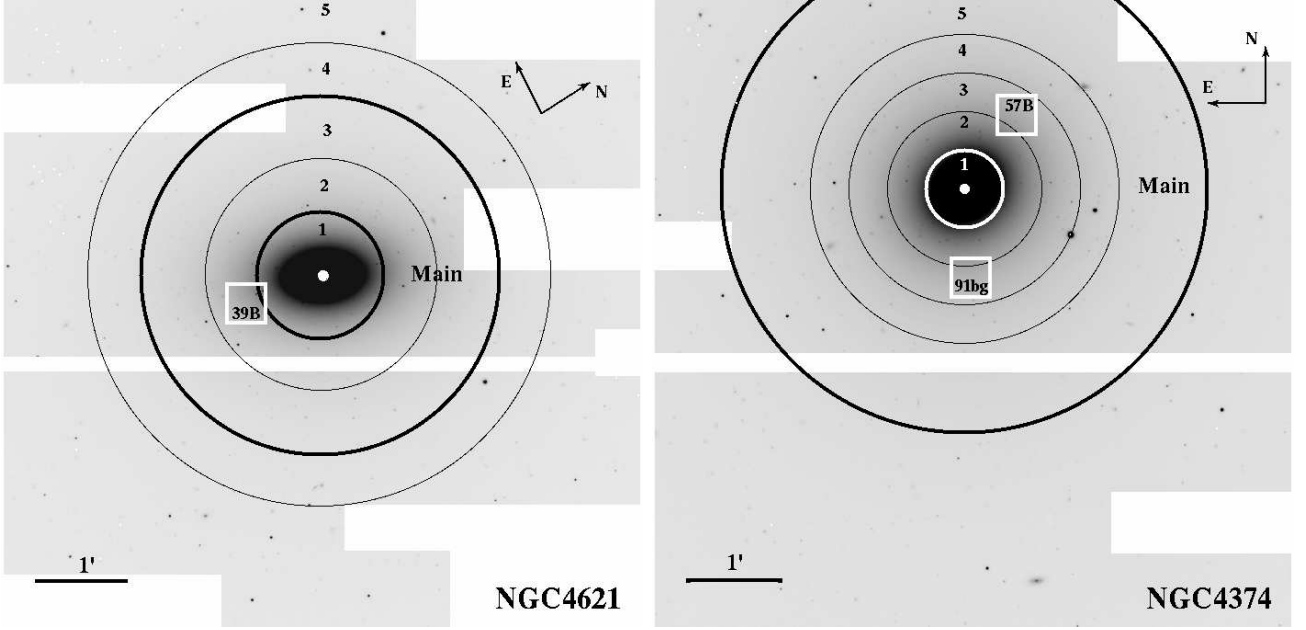


Fig. 1. Left Panel: NGC 4621 *V*-band image with the regions used for SBF and colour analysis. Thick-lined circles mark the borders of the main annulus, thin solid lines show the other annuli (as numbered), white boxes give the location of the SNe (see §2.2). Right panel: as upper, but for NGC 4374 (for sake of clarity the inner border of the main annulus is shown with white colour).

with a Sersic's law (Sersic 1968) plus a constant term. A first model of the galaxy was obtained and subtracted from the sky-subtracted frame. The wealth of bright sources appearing after model subtraction were masked out; the procedure of model fitting and masking was then iteratively repeated until the residual frame (original frame minus galaxy model) was considered satisfactory. After the subtraction of the best galaxy model, the large scale residuals still present in the frame were removed using the background map obtained with SExtractor (Bertin & Arnouts 1996) adopting a mesh size ~ 10 times the FWHM (Cantiello et al. 2005). In the following we refer to the sky, galaxy-model and large scale residuals subtracted image as *residual* frame.

The photometry of fore/background sources and of Globular Clusters (GCs hereafter) was derived with SExtractor on the final residual frame. As described in our previous works, we modified the input weighting image of SExtractor by adding the galaxy model (times a factor between 0.5 and 10, depending on the galaxy; for details see Jordán 2004; Cantiello et al. 2005) so that the SBFs were not detected as real objects. To correct for Galactic reddening we used the $E(B-V)$ values from Schlegel et al. (1998) reported in Table 1. The aperture correction (a.c.) was obtained from a number of isolated point-source candidates in the frames and by making a curve growth analysis out to $6.0''$.

Once the corrected catalogue of sources was derived, the next step was to fit the luminosity functions of external sources, that will be used to estimate the extra-fluctuation term due to unmasked faint sources (Tonry et al. 1990). We derived the fit to GCs and background galaxies luminosity functions from the photometric catalogue of sources, after removing the brightest/saturated point-like sources and the brightest and most extended objects. The best fit of the sum of the two luminosity functions, shown in Figure 2,

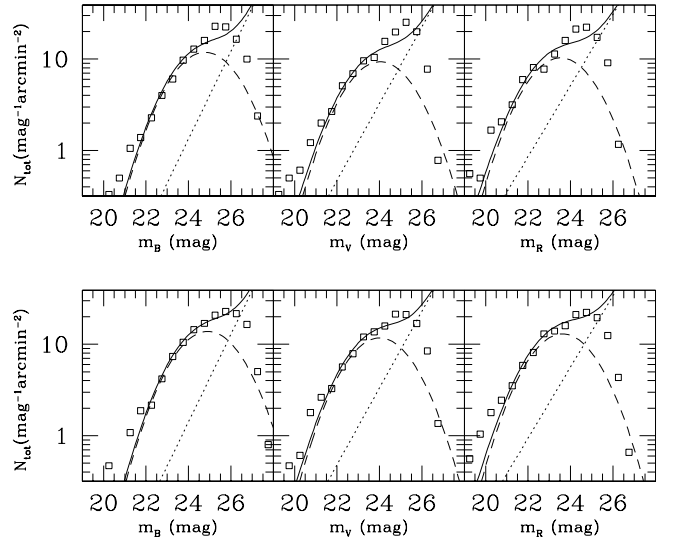


Fig. 2. *B*, *V*, and *R* luminosity functions of external sources in NGC 4621 (upper panels), and NGC 4374 (lower panels). Open squares mark observational data; the solid lines represent the best fit to data. The luminosity functions of background galaxies and GCs are plotted as dotted and dashed lines, respectively.

and the extra-fluctuation correction term, P_r , were derived as in Cantiello et al. (2005).

To measure SBF magnitudes we proceeded by estimating the azimuthal average of the residual frame power spectrum, $P(k)$, then matching it with the power spectrum of a template PSF convolved with the mask image, $E(k)$. The total fluctuation amplitude P_0 was obtained via a robust minimisation method (Press et al. 1992) as

the multiplicative factor required to obtain the matching $P(k) = P_0 \times E(k) + P_1$, where P_1 is the white noise constant term. As template PSF we used 6 different isolated bright point-like sources in each residual frame, which, after normalisation, were singularly adopted to estimate the SBF signal of the galaxy.

For both objects the fluctuation amplitude, $P_f = P_0 - P_r$, was estimated within a circular annulus, adopting the same average inner and outer radii used by Tonry et al. (2001) in order to allow a homogeneous combination of our and Tonry et al. data. Figure 3 shows the power spectrum analysis of both galaxies.

Furthermore, in order to study the radial variation of SBFs, and the SBF properties in the sites where Type Ia Supernova events are recorded, we ran the same SBF measurement procedure described above in five annuli per galaxy, and in three more box-shaped regions centred on each SN. All regions used are shown in Figure 1. We must emphasise that the effect of the extra-fluctuation correction term, P_r , and its relative amplitude with respect to the total fluctuation signal, P_0 , changes from region to region, and the P_r/P_0 ratio increases for outer regions and bluer bands. Thus, a systematic under/over-estimate of P_r may lead to over/under-estimated SBF magnitudes. Table 2 shows the $\langle P_r/P_0 \rangle \times 100$ ratios for all regions and bands considered here; the numbers in the table demonstrate that *V* and *R*-band SBF magnitudes have P_r corrections much lower than the total fluctuation signal, even for the outermost annulus considered. On the contrary, for *B*-band measures the P_r/P_0 ratio in some of the regions considered reaches values as high as ~ 0.45 , implying that the extra correction term is comparable with P_f , thus the SBF magnitudes will be considered with caution in such regions.

Table 3 summarises our measurements; for each galaxy, we tabulate (1) region identification; (2) average equivalent radius of the region $r(arcsec) = \sqrt{(a \cdot b)}$; (3-5) SBF magnitudes measured in *BVR*; (6-7) integrated colours.

3. Analysis of distances

To estimate distances based on the SBF method, as for most distance indicators, a calibration of the absolute SBF magnitude is required. The most widely adopted bands for SBF measures are the optical *I* and *z* bands, and the near-*IR H* and *K* ones (Pahre & Mould 1994; Tonry et al. 2001; Mei et al. 2007; Jensen et al. 2003; Blakeslee et al. 2010). All *z* and *H* measures available come from HST observations taken with the ACS/WFC and NICMOS/NIC2 detectors, respectively (e.g. Jensen et al. 2003; Mei et al. 2007; Blakeslee et al. 2009). The total number of SBF data available in these pass-bands is around ~ 450 measures. As a consequence, the calibrations in such bands, especially the optical ones, are well established as testified, for example, by the accurate characterisation of the \bar{z} versus $(g-z)$ relation derived by Blakeslee et al. (2009) using ACS data of Virgo and Fornax cluster galaxies.

SBF measurements in other bands are not *popular*, with a total of ~ 70 measures available for *B*, *V* and *R* bands (e.g. Tonry et al. 1990; Jerjen et al. 2000; Blakeslee et al. 2001; Sodemann & Thomsen 1996; Cantiello et al. 2007b). This is due to the fact that SBF magnitudes at these wavelengths tend to be more sensitive to stellar population properties and, consequently, the calibration has a larger scatter and is

less reliable, while for distance studies the most favourable condition is that the magnitude of the standard candle is relatively constant or has a tight predictive relation as a function of some other distance-independent property, such as colour. Taking advantage of the well constrained distances of the target galaxies, we will derive new distances based on our measurements and empirical/theoretical calibrations, and compare the various results to test calibrations adopted. In the upper part of Table 4 we report the SBF measures for NGC 4621 and NGC 4374 in different bands as derived in literature, the distance moduli $m - M$, and the calibration used. The second part of the table gives the distances derived by us as discussed below.

3.1. Empirical calibrations

Cantiello et al. (2007a) compared the existing *I* and *V* band calibration equations derived from different observational data, in order to identify the best empirical calibration for the colour interval $0.85 \leq V-I \leq 1.30$ mag in both pass-bands. For *V*-band SBF magnitudes the best calibration equations resulted to be:

$$\bar{M}_V = 0.81 \pm 0.12 + (5.3 \pm 0.8) \cdot [(V-I) - 1.15] \text{ for } 1.05 \leq V-I \leq 1.30 \text{ mag (1);}$$

and

$$\bar{M}_V = -0.50 \pm 0.27 \text{ mag for the } 0.85 \leq V-I \leq 1.05 \text{ mag (2).}$$

To use the above calibration we adopt the *V-I* colours from Tonry et al. (2001), and the SBF measures listed in Table 3 for the main annulus. The distances obtained are shown in Table 4 and will be discussed with all other estimates at the end of the section.

For *R*-band SBF, the most recent empirical calibration for normal elliptical galaxies was provided by Tonry et al. (1990) who, however, considered it unreliable. Distance estimates for a large number of dwarf ellipticals have been provided by Jerjen and collaborators (e.g. Jerjen et al. 1998, 2000, 2004) based on *R*-band SBF measures and semi-empirical relations. Using the *B-R* colour, the authors recognised two different branches for the SBF versus colour relation, a linear branch:

$$\bar{M}_R = -8.94 + 6.09 \cdot (B-R) \text{ for } 1.10 \leq B-R \leq 1.50 \text{ mag (3);}$$

and an parabolic branch, partly overlapping to the previous one:

$$\bar{M}_R = -1.39 + 1.89 \cdot [(B-R) - 0.77]^2 \text{ for } 0.80 \leq B-R \leq 1.35 \text{ mag (4) (Jerjen et al. 2004). To derive distances, reported in Table 4, we used the red/linear branch calibration.}$$

The small amplitude of the fluctuations in the *B*-band and the higher sensitivity to stellar population properties with respect to other optical bands (see, e.g., Worthey 1993a; Cantiello et al. 2003, 2007b) make this band unreliable for distances studies. Besides, only a handful of \bar{B} measures exist, including the present ones, and no distance has been estimated using *B*-band SBF measurements.

3.2. Theoretical calibrations

Empirical calibrations are generally preferred for SBF studies, also thanks to the aforementioned small uncertainties for certain filters. However, the derivation of such relations requires substantial observational effort for each pass-band. On the other hand, models have the advan-

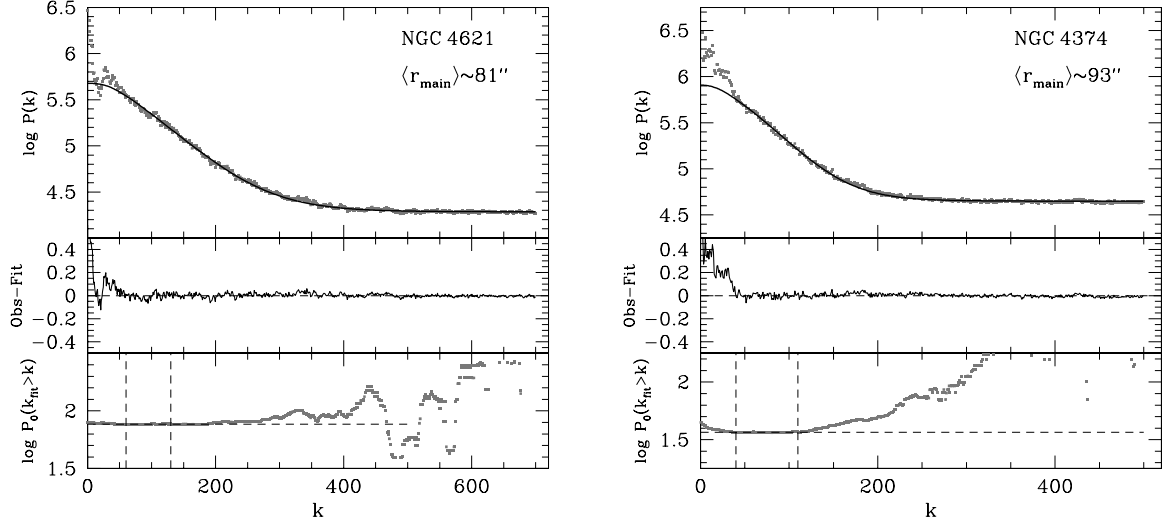


Fig. 3. Power spectrum analysis of the main annuli for both targets. Left panels: NGC 4621 analysis. The upper panel shows the logarithm of the power spectrum of the residual frame (grey dots) and the best fit $P(k)$ curve. In middle panel the difference between observed and fitted data is shown. The flat region of $\log P_0(k_{fit} > k)$ between vertical dashed lines in the lower panel is used to evaluate the best fit parameters P_0 , and P_1 (Cantiello et al. 2005; Biscardi et al. 2008). Right panels: as left, but for NGC 4374.

Table 2. $\langle P_r/P_0 \rangle$ ratios (in %)

	<i>B</i>	<i>V</i>	<i>R</i>	<i>B</i>	<i>V</i>	<i>R</i>
Annulus	NGC 4621			NGC 4374		
Main	17	7	5	29	11	9
1	6	4	4	11	7	8
2	13	6	4	17	9	8
3	24	9	6	26	11	9
4	34	13	8	38	13	9
5	37	15	10	44	16	11
SN 1939B	12	5	4			
SN 1991bg				37	10	9
SN 1957B				25	9	7

Table 3. Surface Brightness Fluctuation and colour measurements corrected for galactic extinction.

Annulus	$\langle r \rangle$ (arcsec)	<i>B</i> (mag)	<i>V</i> (mag)	<i>R</i> (mag)	<i>B</i> − <i>V</i> (mag)	<i>B</i> − <i>R</i> (mag)
NGC 4621						
Main	81	32.83 ± 0.10	31.84 ± 0.06	30.94 ± 0.08	0.893 ± 0.002	1.449 ± 0.002
1	29	32.43 ± 0.09	31.75 ± 0.07	30.96 ± 0.06	0.912 ± 0.001	1.474 ± 0.001
2	58	32.83 ± 0.10	31.83 ± 0.06	30.94 ± 0.08	0.900 ± 0.001	1.455 ± 0.001
3	95	32.83 ± 0.10	31.81 ± 0.06	30.93 ± 0.07	0.884 ± 0.002	1.439 ± 0.003
4	132	32.87 ± 0.11	31.74 ± 0.07	30.90 ± 0.08	0.871 ± 0.005	1.431 ± 0.006
5	193	32.63 ± 0.12	31.59 ± 0.06	30.81 ± 0.06	0.839 ± 0.008	1.391 ± 0.011
SN 1939B	55	33.01 ± 0.10	31.84 ± 0.07	30.97 ± 0.08	0.915 ± 0.001	1.469 ± 0.001
NGC 4374						
Main	93	33.31 ± 0.08	32.11 ± 0.04	31.40 ± 0.08	0.925 ± 0.002	1.494 ± 0.003
1	20	32.43 ± 0.06	31.51 ± 0.04	31.01 ± 0.08	0.945 ± 0.001	1.521 ± 0.001
2	39	33.08 ± 0.07	32.03 ± 0.04	31.33 ± 0.08	0.931 ± 0.001	1.501 ± 0.002
3	63	33.36 ± 0.09	32.23 ± 0.03	31.45 ± 0.08	0.922 ± 0.002	1.489 ± 0.004
4	88	33.58 ± 0.08	32.23 ± 0.02	31.41 ± 0.08	0.919 ± 0.003	1.486 ± 0.006
5	122	33.47 ± 0.10	32.22 ± 0.03	31.44 ± 0.08	0.919 ± 0.006	1.486 ± 0.011
SN 1991bg	58	33.87 ± 0.07	32.13 ± 0.04	31.43 ± 0.08	0.927 ± 0.002	1.495 ± 0.00
SN 1957B	59	33.50 ± 0.09	32.13 ± 0.03	31.35 ± 0.08	0.917 ± 0.002	1.484 ± 0.00

tage of being homogeneous through the different bands, but need many different counter-checks to be considered reliable. In this work we take as reference the SBF versus colour equations derived using the simple stellar population (SSP) models from the Teramo-Stellar Population Tools (SPoT) group³. For a detailed review of the SPoT models we remind the reader to Raimondo et al. (2005) and references therein. These models have already been proved being very effective not only to match the empirical SBF calibrations in different bands, but also to reproduce the resolved (colour magnitude diagrams) and unresolved (colours, magnitudes) properties of stellar populations (Brocato et al. 2000; Cantiello et al. 2003; Raimondo et al. 2005; Cantiello et al. 2007a; Biscardi et al. 2008; Cantiello et al. 2009; Raimondo 2009).

For example, in a previous paper, Biscardi et al. (2008) showed that the SPoT models for an age interval between 1.5 and 14 Gyr, and metallicity $[Fe/H]$ between -0.4 and 0.3 dex are able to reproduce both the *I*-band and *z*-band calibrations from Tonry et al. (2001) and Mei et al. (2007), respectively.

In the present work we adopt the same models used by Biscardi et al. and derive absolute *V* and *R*-band SBF magnitudes versus the integrated *B*–*R* colour. Using the on-line SPoT models we obtain the following relations:

$$\bar{M}_R = -4.11 + 2.84 \cdot (B-R) \quad (5),$$

$$\bar{M}_V = -2.69 + 2.60 \cdot (B-R) \quad (6),$$

we also derive, for sake of completeness, the *B*-band calibration:

$$\bar{M}_B = -0.68 + 2.32 \cdot (B-R) \quad (7).$$

However, we recall that it is hazardous to derive distances from eq. (7) because \bar{M}_B strongly depends on the properties of the stellar population originating the SBF signal (see section § 4.1).

As a further check based on an independent set of stellar population models, we also used the *V* and *R* equations provided by Blakeslee et al. (2001), which, differently from the SPoT models, are derived using composite stellar populations (see the quoted paper for more details).

The distance moduli of the two targets, obtained using both the SPoT and the Blakeslee et al. (2001) theoretical calibrations, are reported in Table 4.

3.3. Results

By inspecting the new and old distance estimates in Table 4 we find a satisfactory agreement within the quoted uncertainties, no matter what calibration (empirical or theoretical) or pass-band/colour relation is used, with the sole exception of *B*-band data which we report here only for sake of completeness.

The distance moduli derived from SBF are affected by the uncertainties present in the empirical/theoretical calibrations, besides the uncertainty of the SBF measure itself. In this work, for the distance moduli taken from literature where no calibration error is given we consider safe to assume an error of the order of ~ 0.20 mag, which includes zero-point uncertainty and the scatter of empirical calibrations (Tonry et al. 2001; Jensen et al. 2003). Similarly we assume ~ 0.20 mag error for the theoretical calibrations, which is originated by the spread between models with different age and metallicity.

Keeping in mind such uncertainty, and the error in the SBF measures, the results in Table 4 can be summarised as follows:

- although the colour provided by Tonry et al. was measured in galaxy regions slightly different from ours⁴ the distances derived from \bar{V} using eq. (1) agree with other data from literature. A similar result is true for \bar{R} if the linear branch relations by Jerjen et al. (2004) are adopted;
- the distance estimates obtained using empirical calibrations show a slight tendency to have a smaller scatter with respect to those from theoretical calibrations;
- whether SSP models from the SPoT group or the Blakeslee et al. (2001) composite models are used the distances derived are substantially similar to each other, and agree with expected values. Such result implies that for the bandpasses and the colour interval considered here composite stellar population models, which try to better reflect the real population mixing of galaxies, are not strictly necessary for the purposes of deriving appropriate SBF versus colour relations;
- as discussed above, coupling \bar{B} measures with eq. (7) provides unreliable distance moduli, this confirms that this band must be discarded for distances. Interestingly, the difference between the *B*-band distance moduli and the literature average moduli is significantly larger for NGC 4621 ($\Delta(m-M) = (m-M)_{B,SBF} - \langle m-M \rangle_{lit.} \sim -0.8$ mag) than for NGC 4374 ($\Delta(m-M) \sim -0.6$ mag). We will analyse further this evidence in the next section on stellar population analysis.

Finally, the last lines of Table 4 provide the median distance moduli of the two targets obtained by averaging *i*) our estimates (empirical and theoretical calibrations, except *B*-band), *ii*) all SBF $m-M$, including ours, *iii*) the distance moduli without SBF⁵, and *iv*) the results from ours plus all literature data. By inspecting such data we find an excellent agreement between our and literature distance moduli and, more in general, between non-SBF and SBF-based distances, a results that should be regarded as a direct evidence of the absence of any significant bias or systematics between the quoted distances. In addition, such agreement also proves the reliability of *V*- and *R*-band SBF calibrations presented in this section.

3.4. Comparison with SNe Ia distances

The comparison of SBF and SNe Ia distances plays a fundamental role in the problem of the cosmological distance scale. SBF magnitudes are capable of providing distances with $\lesssim 10\%$ accuracy within 100 Mpc (Jensen et al. 2001; Biscardi et al. 2008; Blakeslee et al. 2010), a result that will

⁴ As explained before, we adopted the same “average” inner and outer radii of Tonry et al., but the detailed shape of the annulus, plus the masking of sources is clearly different between the two datasets.

⁵ All non-SBF distances are taken from the NED Redshift Independent Distance database. The distance indicators used include Globular Cluster and Planetary Nebulae Luminosity Functions, Type Ia Supernovae and Globular Cluster half light radii. For a complete list of methods, and associated references, visit the URL <http://ned.ipac.caltech.edu/forms/d.html>. In case of multiple estimates obtained with the same indicator only the most recent one is considered.

³ Visit the web-site: www.oa-teramo.inaf.it/spot

Table 4. Galaxy distances from this work and from literature.

Filter	Colour	Ref. Color/Data	NGC 4621		NGC 4374	
			\bar{m}	$m - M$	\bar{m}	$m - M$
SBF from literature						
<i>I</i>	<i>V-I</i>	[1]	29.67± 0.18	31.16±0.20	29.77± 0.09	31.16±0.11
<i>z</i>	<i>g-z</i>	[2]	29.12 ^a ± 0.01	30.86±0.07	29.53 ^a ± 0.01	31.34±0.07
<i>K</i>	...	[3]	25.46± 0.16	...	25.43± 0.22	...
Our measurements						
Empirical Calibrations ^b						
<i>V</i>	<i>V-I</i>	[4]	31.84± 0.06	30.91±0.21	32.11± 0.04	31.08±0.20
<i>R</i>	<i>B-R</i>	[5]	30.94± 0.08	31.05±0.21	31.40± 0.08	31.25±0.22
Theoretical Calibrations-SSP ^b						
<i>B</i> ^c	<i>B-R</i>	[6]	32.83 ±0.10	30.2	33.31 ±0.08	30.5
<i>V</i>	<i>B-R</i>	[6]	31.84 ±0.06	30.76±0.21	32.11 ±0.04	30.91±0.20
<i>R</i>	<i>B-R</i>	[6]	30.94 ±0.08	30.93±0.21	31.40 ±0.08	31.27±0.22
Theoretical Calibrations-CSP ^b						
<i>V</i>	<i>V-I</i>	[7]	31.84± 0.06	30.99±0.21	32.11± 0.04	31.17±0.20
<i>R</i>	<i>V-I</i>	[7]	30.94± 0.08	31.04±0.21	31.40± 0.08	31.41±0.22
Median $m - M$						
			NGC 4621		NGC 4374	
This work			30.96 ±0.11		31.21± 0.17	
all SBFs			31.08 ±0.19		31.21± 0.14	
No SBFs			30.97 ±0.21		31.17± 0.18	
All available $m - M$			30.98 ±0.17		31.22± 0.16	

References

- [1] Tonry et al. (2001); [2] Blakeslee et al. (2009); [3] Pahre & Mould (1994); [4] Cantiello et al. (2007a); [5] Jerjen et al. (2004); [6] this work; [7] Blakeslee et al. (2001).

Notes

^a Blakeslee et al. (2009) data are given in the AB-mag system.

^b We adopted ~ 0.2 mag as safe calibration error for *i*) distance moduli given in literature with no calibration uncertainty, and *ii*) distances based on theoretical calibrations (see text).

^c Distances derived from *B*-band SBF are reported to show that the sensitivity of \bar{B} to stellar population properties makes unreliable any distance estimate.

be likely improved with new and next generation observing facilities, allowing to estimate accurate distances of bright ellipticals out to ~ 200 Mpc. On the other hand, SNe Ia can provide distances to objects at much larger distances. Thus, deriving self-consistent distances using these two indicators is a crucial step to bridge local to cosmological distances, in order to reduce the number of rungs in the cosmological distance scale, i.e. to reduce systematic uncertainties.

The sample of objects with known SBF measures and well studied SNe Ia light curves is relatively small, due to the fact that SNe Ia occur in all kind of galaxies, but are mostly observed in late type galaxies because of an observational bias, on the contrary SBF are measured almost only in early type galaxies.

Nevertheless, a comparison of SBF and SNe Ia distances was carried out by Ajhar et al. (2001), who found that there is a good agreement between the two distance indicators, provided that a consistent set of Cepheid calibrating galaxies is used. However, their statistics grounded on ~ 10 objects and Ajhar et al. made it clear that “[...] Unquestionably, the SNIa and SBF absolute calibrations are in need of further refinement.”

As already mentioned, a total of three type Ia Supernova events has been recorded in the two galaxies. Two SN Ia have been observed in NGC 4374, SN 1991bg and SN 1957B, while SN 1939B was discovered in NGC 4621. The SNe are

located all at ~ 1 arcmin from the photometric centre of the host galaxy. Even though all three SNe are classified as type Ia, they show a wide range of luminosity – not unexpected in E/S0 galaxies (Gallagher et al. 2005) –, in particular all events are fainter at maximum light than a normal SN Ia after correcting for the correlation between peak luminosity and decline rate (Hamuy et al. 1996). SN 1991bg is one of the most sub-luminous SNIa yet observed (~ 2.5 mag fainter than normal, Turatto et al. 1996). SN 1957B has an absolute magnitude at maximum ~ 0.2 mag fainter than a normal SN, but still brighter than SN 1991bg (Howell 2001). Finally, SN 1939B at maximum light is ~ 0.6 mag sub-luminous (Minkowski 1964).

Unfortunately, being sub-luminous events, the standard peak luminosity versus decline rate relation does not provide good distance estimates with these SNe. Ajhar et al. (2001), in fact, did not take into account SN 1939B and SN 1957B, while SN 1991bg appeared in their list of Supernovae but it was not used for SBF-SNe Ia comparison, it is was instead included “for completeness and for future studies of SNe Ia luminosities.”

More recent studies, however, have provided new methods that can be adopted to derive distances with these sub-luminous SNe: the calibration based on decline rate and colours by Folatelli et al. (2010), the MLCS2k2 by

Jha et al. (2007), and the ΔC_{12} method by Wang et al. (2006).

Using eq. (6) of Folatelli et al. (2010) with the best-observed fit parameters, we obtain the following distance moduli:

- SN 1939B in NGC 4621: taking the peak luminosity from the Asiago Supernova Catalogue (Barbon et al. 1989)⁶ $m_{B,max} = 12.3$, a decline rate of $\Delta m_{15} \sim 1.75$ estimated from the light curve reported in Leibundgut et al. (1991), and using eq. (3) from Folatelli et al. (2010) to get the $(B^{max} - V^{max})_0$ colour, we obtain $m - M = 31.0$, with an uncertainty of the order of ~ 0.5 mag if errors of ~ 0.2 mag, 0.25 days and 0.15 mag are adopted for $m_{B,max}$, Δm_{15} and $(B^{max} - V^{max})_0$, respectively;
- SN 1957B in NGC 4374: adopting $m_{B,max} = 12.20 \pm 0.14$ (Lanoix 1998), $\Delta m_{15} = 1.3$ (Howell 2001), and $(B^{max} - V^{max})_0 = 0.01$ (using eq. (3) from Folatelli et al. 2010) the distance modulus is $m - M = 31.1$, with uncertainty ~ 0.3 mag adopting an error of ~ 0.1 on both the decline rate and on $(B^{max} - V^{max})_0$;
- SN 1991bg in NGC 4374: with $m_{B,max} = 14.75$ and $m_{V,max} = 13.95 \pm 0.02$ (Turatto et al. 1996), $\Delta m_{15} = 1.93 \pm 0.10$ (Phillips et al. 1999) we derive $m - M = 31.1 \pm 0.3$;

In all cases the distance moduli derived using the calibration from Folatelli et al. (2010) agree within uncertainties with the median values reported in Table 4.

Jha et al. (2007) developed an updated version of the MLCS method (Riess et al. 1998) called MLCS2k2, which includes new procedures for the K -correction and for internal extinction corrections. Using the light curve parameters of SN 1991bg Jha et al. derive $m - M = 31.42 \pm 0.10$ adopting $H_0 = 65 \text{ Km s}^{-1} \text{ Mpc}^{-1}$. Although such distance agrees with the values reported in Table 4, the agreement becomes certainly better if $H_0 = 73 \text{ Km s}^{-1} \text{ Mpc}^{-1}$ is taken - a value consistent with the ones typically derived from SBF distances (Tonry et al. 2000; Freedman et al. 2001) - as suggested by the authors; in that case, in fact, one has $m - M = 31.17 \pm 0.10$ mag.

In the case of Wang et al. (2006) the calibration parameter adopted is the ΔC_{12} , i.e. the $B - V$ colour at 12 days past optical maximum. The authors find $m - M = 30.35 \pm 0.19$, based on the properties of SN 1991bg and using $H_0 = 72 \text{ Km s}^{-1} \text{ Mpc}^{-1}$. Such $m - M$ is more than $2 - \sigma$ out the median values in Table 4 obtained using many independent distance indicators, and it also disagrees with the values obtained using the Folatelli et al. (2010) or Jha et al. (2007) calibrations, thus we flag the Wang et al. estimate as unreliable for the case of SN 1991bg.

In conclusion, we find that the distances of NGC 4621 and NGC 4374 derived via the light curve properties of their SN Ia agree perfectly with the SBF distances - and with the most recent estimates from literature - if the calibration by Folatelli et al. (2010, useful for all three SNe), or Jha et al. (2007, for the case of SN 1991bg) are used.

4. Analysis of unresolved stellar populations with SBF and integrated colours

As mentioned before, the SBF magnitude of a stellar population corresponds to the ratio of the second to the first moment of its luminosity function. Since its first applications, such characteristic has suggested the use of the SBF method as a powerful diagnostics of stellar population properties. The earliest theoretical studies on this subject (Buzzoni 1993; Worthey 1993a,b) were focused on the relationship between SBF and age/metallicity, but also showed how the fluctuation amplitude in bluer pass-bands, like B , could be used as a useful tracer of the hot stellar components in the galaxy. Despite several authors have confirmed, and further extended, such early findings (Blakeslee et al. 2001; Cantiello et al. 2003; González et al. 2004; Raimondo 2009), a comprehensive and homogeneous analysis of multi-band SBF measurements for a large sample of galaxies is still missing. The various set of models have clearly shown that optical to near- IR SBF colours can be very effective to lift the age/metallicity degeneracy which affects “classical” integrated colours (Worthey 1994). Observationally, a few $\bar{I} - \bar{H}$ data exist in literature (Jensen et al. 2003), but they mostly refer to spatially non homogeneous regions. On the other hand, $\bar{V} - \bar{I}$ colours have also been studied for various galaxies, but they suffer for an age/metallicity degeneracy similar to classical colours, although the information obtained using such measures is independent and complementary to the integrated colours derived for the same targets (Tonry et al. 1990; Blakeslee et al. 2001; Cantiello et al. 2007a,b).

Concerning the use of SBF to study stellar populations, using high quality data has allowed to measure SBF variations in optical bands within different regions of the galaxy. As a consequence, even if V and I SBF magnitudes and colours are not as much effective in removing the age/metallicity degeneracy (see below), the measure of SBF radial variations has provided useful results on how the mean properties of the dominant stellar population change with galactic radius (Cantiello et al. 2005).

The targets analysed in this work have already been considered for other SBF measurements surveys. In particular, the aforementioned ground-based SBF survey (Tonry et al. 2001), the near- IR measurements for nine Virgo ellipticals by Pahre & Mould (1994), and the ACS Virgo Cluster Survey (Côté et al. 2004) all have the two galaxies in their target list. The SBF magnitudes from these databases are reported in the first part of Table 4. None of these cited works presents the measurement of SBF magnitudes at various galactic radii. On the contrary, thanks to the high quality of the VLT data available, we have been able to obtain fluctuation amplitudes at various radii (Table 3).

Differently from other bright elliptical galaxies studied in previous works (Cantiello et al. 2005, 2007a), we can report the absence of radial \bar{V} and \bar{R} gradients in NGC 4374. For NGC 4621, instead, a small but non-negligible brightening of SBF magnitudes at larger radii is found in V and R . On the other hand, the \bar{B} of both galaxies shows a significant scatter between the different annuli, thus no evidence of systematic trends with radius is observed in this band.

⁶ The updated catalogue is available at the URL <http://graspa.oapd.inaf.it>

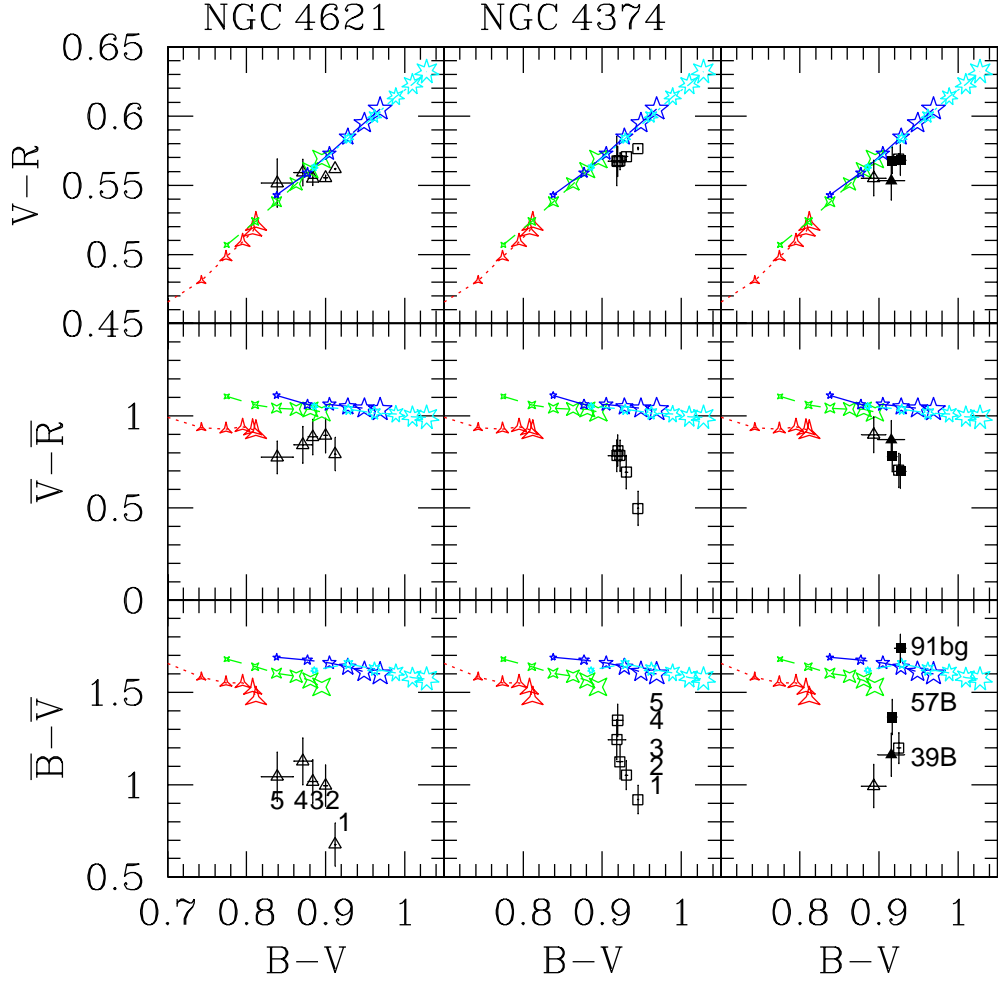


Fig. 4. SBF-colours and integrated-colours measured for NGC 4621 (left panels) and NGC 4374 (middle panels), compared to the SPoT models from Raimondo et al. (2011). Black symbols mark observational data for the various annuli as labelled (triangles for NGC 4621, squares for NGC 4374). Measures within regions hosting SNe, and the measure for the main annulus for both galaxies are shown in right panels: NGC 4621 and its SN Ia (SN 1939B) are shown with a full and empty triangle, respectively; NGC 4374 and its SNe Ia (SN 1957B, and SN 1991bg) are shown with full and empty squares, respectively. For the models, different $[Fe/H]$ are indicated with different symbols ($[Fe/H] = -0.7, -0.4, 0.0, +0.4$ dex with three, four, five and seven pointed stars, respectively). Larger symbols size mark older ages, from 4 to 14 Gyr with 2 Gyr step. [See electronic version of the Journal for a colour version of the figure.]

4.1. SBF-colours versus integrated colours

By plotting SBF and integrated colours for each target (Figure 4), and comparing the data of the two galaxies between them and with models, we can make various considerations on the host unresolved stellar systems. We consider the updated version of the SPoT models (Raimondo et al. 2011), which for the photometric bands and chemical composition used in this section confirm the results obtained from the previous Raimondo et al. (2005) models.

As a first general consideration, we find that the SBF $\bar{V}-\bar{R}$ colour, and the integrated $B-V$ and $V-R$ colours predicted by models representing old ($\gtrsim 7$ Gyr) and metal rich ($[Fe/H] \gtrsim -0.4$ dex) SSPs are in good agreement with the measured values. Differently, the \bar{B} is much more sen-

sitive to the properties of the dominant stellar population (see below) and the matching with “canonical” SSP models is less satisfactory in this band.

Starting from these general considerations on the properties of the “dominant” stellar population in the galaxies (i.e. the stellar population which is emitting the largest part for the flux responsible for the colours and the SBF signal) let us analyse more in details the result of Figure 4.

The left and middle columns of panels in Figure 4 show the SBF colours and $V-R$ measurements in the five annuli considered for each galaxy versus the integrated $B-V$. The annuli appear numbered in the lower panels according to the numbers reported in Table 3, so that inspecting the data in the figure it is also possible to recognise the radial behaviour of plotted quantities. In the third column, instead,

the overall SBF measures are plotted (“main” annulus data in Table 3, empty symbols) together with SBF in the SNe regions. It is useful to emphasise that for both galaxies our integrated colours and colour profiles agree with the same measurements from Idiart et al. (2002).

By inspecting results in the figure, we find that NGC 4621 does not show any significant SBF colour gradient either in $\bar{B}-\bar{V}$ or $\bar{V}-\bar{R}$ (lower and middle left panels), and no gradient even in the integrated $V-R$ colour (top left panel). The only colour showing radial changes is the $B-V$, varying from ~ 0.91 mag for the inner annulus (#1), to ~ 0.84 in the outermost (#5). As already mentioned, inspecting the \bar{V} and \bar{R} data for NGC 4621 in Table 3, a small but non-negligible gradient seems to be present, of ~ 0.25 mag in V and ~ 0.15 mag in R , if the inner annulus is discarded. The \bar{V} and \bar{R} gradients have the same trend with colour, i.e. brighter SBF magnitudes associated with bluer colours/larger radii, thus they tend to cancel-out when the SBF-colour is considered. In fact, if the innermost annulus is neglected, a SBF-colour gradient of appears in the $\bar{V}-\bar{R}$ versus $B-V$ plane for NGC 4621, although it is of the same amplitude of estimated uncertainties. Even so, the radial trends of the SBF magnitudes and of the $B-V$ are both consistent with the well known scenario of a more metal-poor stellar component (i.e. bluer integrated colours, and brighter SBF magnitudes for the pass-bands considered here) at larger galactocentric radii.

For NGC 4374 (central panels) we find that $\bar{V}-\bar{R}$ and $V-R$ are practically flat along the galaxy radius, if the innermost annulus (#1) is excluded. Due to the presence of a dusty disk in the galaxy centre, in fact, we left unmasked only a small fraction of the area in the annulus #1, but further contamination from dust might still be present. Differently from the previous case, the V and R data of NGC 4374 in Table 3 do not show any systematicity versus radius, although the $\bar{V}-\bar{R}$ versus $B-V$ panel seems to show a correlation between the two plotted magnitudes, mostly due to the cited innermost annulus.

As mentioned above, the comparison between measurements and models in the two upper panels of each column reveals that the data of galaxies lie close to the position of SSPs with $[Fe/H] \gtrsim -0.4$ dex and $t \gtrsim 7$ Gyr. However the age-metallicity degeneracy suffered by classical and SBF colours obtained by combining these bands prevents us from giving more precise information on the dominant stellar components in the galaxy.

The lower panels, which involve \bar{B} , deserve a separate and detailed discussion, since both galaxies show a $\bar{B}-\bar{V}$ colour much bluer than models, an evidence more severe for NGC 4621. For this galaxy, in fact, the $(\bar{B}-\bar{V})_{Main}$ is ~ 0.2 mag bluer than NGC 4374, and ~ 0.4 mag bluer than models. We also note that NGC 4374 shows a radial change leading the $\bar{B}-\bar{V}$ value of the outermost annulus to be quite similar to the models. Differently, NGC 4621 does not present any systematic gradient and, except for the innermost annulus the $\bar{B}-\bar{V}$ is nearly constant in every studied region of the galaxy.

To understand the origin of the mismatch between data and models, visible in the lowermost panels of Figure 4, and of the peculiarly blue $\bar{B}-\bar{V}$ colour of NGC 4621, we have considered to take advantage of the versatility of the SPoT stellar population synthesis code and carry out some specific numerical simulations, to investigate if and how the presence of a complex stellar population modifies the ex-

pected $\bar{B}-\bar{V}$. In addition, for metal rich models we have also considered the case of a non negligible fraction of Horizontal Branch (HB) stars having higher effective temperatures with respect to “canonical” stellar evolution models.

In order to find indications on the origin of the peculiar $\bar{B}-\bar{V}$ behaviour of the two galaxies, our numerical tests have been organised as follows: 1) we have explored the effects of the presence of a hot HB (HHB) component to field stars; 2) a young stellar population is added to a “reference” old and metal-rich population, and 3) a metal-poor population is added to the reference one. For the comparison in B , V and R bands we adopted the SBF measured in five annuli, plus the measures in the SNa Ia regions, while for the panels including the \bar{K} taken from literature we adopted our main annuli SBF measurements. The results of the simulations and the comparisons with data are briefly discussed below, and shown in Figure 5 where three different SBF colours are plotted against $B-V$.

- In order to mimic the presence of HHB stars, we carried out a numerical experiment by considering that 50% of HB stars have suffered large mass-loss during the RGB phase (first column of panels in Figure 5). As a result, a percentage of low mass stars populates the blue/hot part of the horizontal branch. This is not unrealistic since such hot component is observed in several metal-rich stellar clusters (e.g. NGC 6441 and NGC 6388), whatever the mechanism responsible of this evidence is. In the figure we consider three populations with solar metallicity and ages 10, 12, and 14 Gyr. Both SBF and integrated colours move from the “standard” positions (standard HB, SHB, label in the figure) to the hot/blue region of the diagram (HHB in the figure). The effect is larger for SBF colours including \bar{B} with respect to integrated colour due to their increased sensitivity to even a small number of bright hot stars.
- In the second numerical experiment (middle panels) a very young population (two different ages are considered: 30 Myr and 100 Myr) is added to a population of 14 Gyr and solar metallicity, with mass ratio between the two components $1_{old} : 10^{-3}_{young}$. From the middle panels of Figure 5 appears that a very recent and *diffuse* burst of star formation is required to obtain a good matching between models and data.
- The third column of Figure 5 reports the effects of a secondary metal-poor component of 14 Gyr added to the main solar metallicity one, the $[Fe/H]$ of the metal-poor component are labelled in the lower right panel of the Figure. Only a very metal poor population with a mass comparable to the one of the main component ($1_{m.rich} : 1_{m.poor}$) produces relevant effects on SBF colours. In that case, however, the values of the observed integrated colour $B-V$ are not well reproduced any more.

The three sets of simulations described seem to point out what already suggested: the most likely solution to the puzzling behaviour of B -band SBF is the presence of hot HB stars. In fact, while the presence of a hot/young stellar component provides a good matching between integrated and SBF colours models with data (second scenario, middle panels in Figure 5), it appears unrealistic that these regular ellipticals host such diffuse and very young stellar component. Moreover, in such a case, i.e. an object with massive

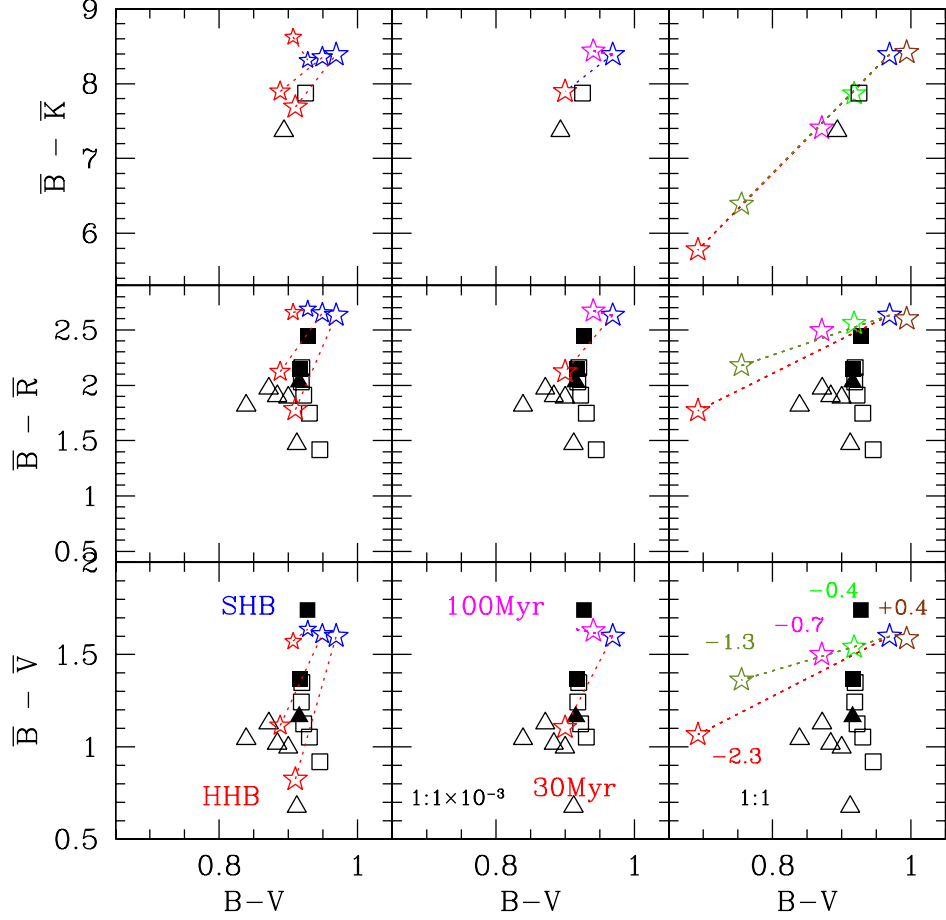


Fig. 5. SPoT stellar population models obtained with non-canonical assumptions. In all cases the initial (standard) population has solar metallicity and $t \sim 14$ Gyr, and is shown with a blue star in each panel, while the final composite population is shown with a different colour and connected with a dashed line to the reference model. Upper panels show main annulus measures, middle and lower panels show multi-annuli measures and SNe Ia regions. Left panels: a fraction equal to 50% of the total HB-stars is simulated being HHB. For these models three ages are considered ($t=10, 12$ and 14 Gyr, increasing ages are marked with larger symbols). Middle panels: a young population of $t=30$ Myr (red), or $t=100$ Myr (magenta) is added to the old solar one. The fraction in mass of old to young stars is reported in the lower panel. Right panels: various metallicities are added to the solar one, as labelled. The mass fraction metal-poor to standard SSPs is shown in the lower panel. Symbols for observational data are as in Figure 4. [See electronic version of the Journal for a colour version of the figure.]

and extended recent star formation, it is likely that a large quantity of dust would still be present, preventing the SBF measure itself. However, with the only exception of an inner $r \lesssim 20''$ dust ring in NGC 4374, we do not find any sign of extended dust in both galaxies. The two-metallicity mixing scenario seems even more unlikely, such mixing, in fact, does not solve the mismatch between data and models for optical bands.

As a further element in support of the role played by HHB stars in determining the SBF signal of NGC 4621, we recall the works by Brown et al. (2000) and Brown et al. (2008), based on deep near and far-UV images of the compact elliptical galaxy M 32. Using HST data, the authors

found that the number of PAGB stars in M 32 is significantly lower than the expectations of their stellar evolution models, while the presence of a HHB population has been observed and identified as the main contributor to the UV-emission of the galaxy.

Related to this issue, Cantiello et al. (2007a), using the \bar{B} data of eight ellipticals, suggested that the role of hot evolved stars cannot be neglected in modelling SBF magnitudes in this pass-band. In that case, though, the mismatch between the data and models in \bar{B} was solved by enhancing the number of PAGB expected assuming the evolutionary prescriptions by Brocato et al. (1990) and Brocato et al. (2000).

As far as concerns NGC 4621, our present results point towards the direction suggested by the observations of M 32. We show that HHB stars can be the stellar component responsible of the observed \bar{B} -excess, even though a combination of two stellar components (HHB and PAGB stars) could not be ruled out and the topic requires further investigations.

As already mentioned for the case of M 32, a further piece of information comes from the comparison of the integrated properties of the two galaxies in the wavelength interval where the very hot stellar component is dominant, i.e. the *UV* regime. In this wavelength regime, Longo et al. (1991) found that NGC 4621 is brighter than NGC 4374. The puzzling presence of a strong *UV* emission in some regular early-type galaxies, discovered in late '70s (Code et al. 1972; Bertola et al. 1980), is now widely interpreted as the presence of a old hot stellar component. Although the mechanisms that created such component, or its true nature, are not well understood (Park & Lee 1997; Kaviraj et al. 2007; Han 2008), some of these old hot stellar sources may have effects on \bar{B} , as discussed by various authors based on both SSP models predictions (Worthey 1993a; Cantiello et al. 2003), or on empirical data (Shopbell et al. 1993; Sodemann & Thomsen 1996; Cantiello et al. 2007a). Moreover, a recent study of Buzzoni & González-Lópezlira (2008) presented a detailed analysis on the link between the *UV* characteristics and near-*IR* SBF amplitudes of elliptical galaxies.

In conclusion, the present analysis seems to support a scenario where the peculiar $\bar{B}-\bar{V}$ is related to a hot and old diffuse stellar component, like HHB stars. Larger samples of SBF colours in blue bands are required to provide further constraints.

4.2. SBF colour-colour diagrams

The coupling of literature *I*, *z* and *K*-band SBF data for the two galaxies with our measures (main annuli) provides a sample of six independent SBF values useful to obtain three independent SBF-colour versus SBF-colour diagrams. Such wide pass-band coverage is, to our knowledge, the first ever presented for SBF. The diagrams with observations are shown in Figure 6, together with models. The upper panel of the Figure shows a feature that has already been discussed (e.g. Blakeslee et al. 2001; Cantiello et al. 2003), that is that model separation for pure optical SBF colours is not effective in removing the age-metallicity degeneracy. In such panel, in fact, all $[Fe/H] \geq -0.4$ dex models overlap to each other, with old and metal rich models superposed to young and metal poor ones.

The models degeneracy is significantly reduced in the middle panel, which includes the optical to near-*IR* $V-K$ SBF colour. The position of the two objects overlaps with models with different metal contents. In particular the bluer point, i.e. NGC 4621, is located near to the region of $[Fe/H] \sim -0.4$ dex with respect to NGC 4374, which appears slightly more metal-rich. Such behaviour is not unexpected, since the latter galaxy is brighter than the first one and, due to the known mass-metallicity relation (e.g. Bernardi et al. 1998), it is reasonable to expect a field population slightly more metal-rich in NGC 4374. It is worth to emphasise that the two-SBF-colour panel represents a useful tool to provide insights to the “absolute” $[Fe/H]$ of

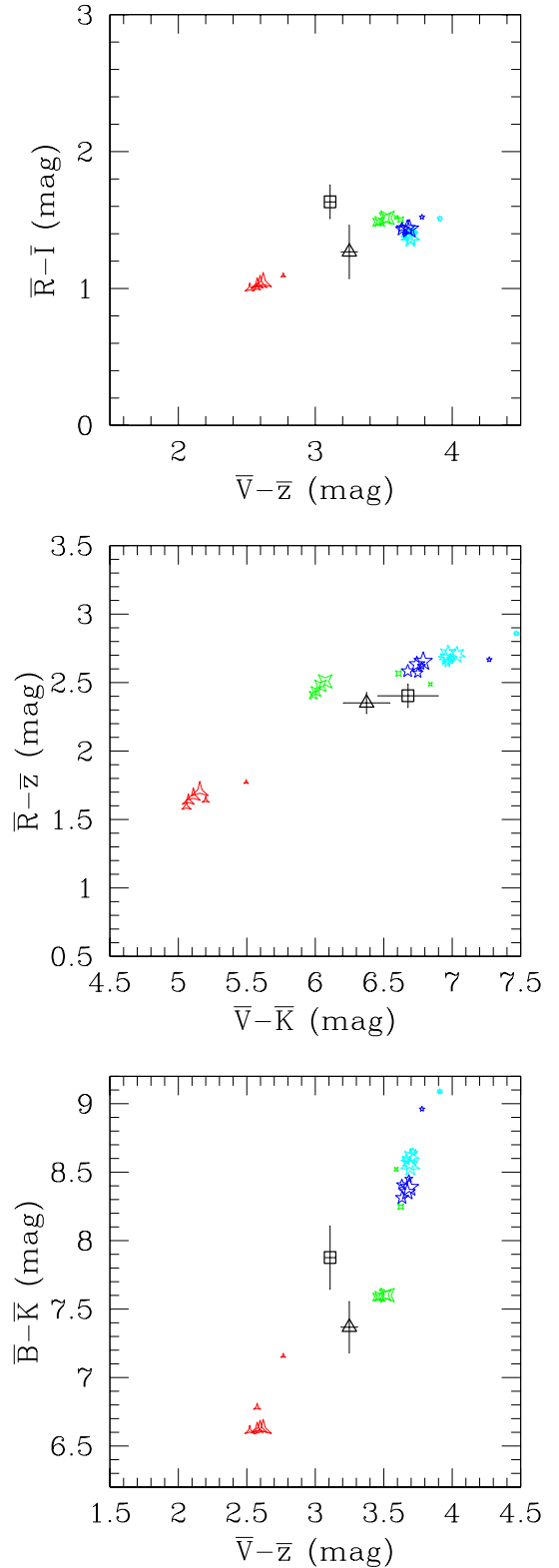


Fig. 6. SBF colour-colour diagrams obtained from present measures (main annulus) and literature data. Symbols and models are the same as for Figure 4. For consistency with other filters the *z*-band SBF magnitudes given by Blakeslee et al. (2009) are transformed from the ABmag to the Vegamag system according to Sirianni et al. (2005). [See electronic version of the Journal for a colour version of the figure.]

the dominant stellar component, within the observational error-bars, and the SSP models scenario adopted.

In other words, based on the SBF-colours analysis and on the integrated colours of field stars from this work (see also Tonry et al. 2001; Idiart et al. 2002; Mei et al. 2007) we find that the dominant stellar population of NGC 4374 is either more metal rich or older, or both, than what found in NGC 4621. Moreover, this result agrees with independent estimates of the metal content in these galaxies, based on spectral index measurements, which predict nearly identical (Idiart et al. 2007) or slightly higher metallicity for NGC 4621 (Kuntschner et al. 2001; Scott et al. 2009).

It must be pointed out, though, that these results are based on the naive interpretation of field stellar population properties solely in terms of age and chemical content differences. Nevertheless, as discussed above, SBF magnitudes and colours can be very sensitive to the presence of a blue/hot stellar sub-system, especially SBF in bluer pass-bands.

The lower panel in Figure 6 includes our \bar{B} measurements. As for the first panel, the $\bar{V}-\bar{z}$ colour is used in abscissa, in this case the separation between different SSP models allows to recognise that for the two larger $[Fe/H]$ values the $\bar{V}-\bar{z}$ colour is bluer for older ages. Taking as reference the models with solar metallicity, one can conclude that both galaxies have similar $\bar{V}-\bar{z}$, matching with the oldest SSP models, but NGC 4621 has $\bar{B}-\bar{K} \sim 0.6$ mag bluer than NGC 4374, as one would also expect in the case of a diffuse hot stellar component is present in this galaxy. As an example, a canonical SSP model at $t = 14$ Gyr, solar metallicity has $\bar{B}-\bar{K} \sim 8.4$ and $\bar{V}-\bar{z} \sim 3.7$ mag; by artificially increasing the number of HHB stars (as described in section 4.1) our models predict $\bar{B}-\bar{K} \sim 7.7$, i.e. roughly the $\Delta\bar{B}-\bar{K}$ colour difference between the two galaxies, while $\bar{V}-\bar{z}$ is left unchanged.

A further consideration is the fact that in the bottom panel of Figure 6, NGC 4621 falls within the region of models with $[Fe/H]$ between -0.7 and -0.4 dex, even though the B -band SBF is too bright. Such behaviour could be explained with bright K -band SBF, so that the B and K SBF excess compensate each other allowing observations to match with models of intermediate metallicity. This would also make $\bar{V}-\bar{K}$ too red, causing the shift observed in the middle panel. In that case, i.e. too bright B and K -band SBF, the three panels of Figure 6 are all suggesting a $[Fe/H] \lesssim -0.4$ for NGC 4621, and a larger metallicity for the dominant stellar component in NGC 4374.

Whether the position of NGC 4621 with respect to models is due to the presence of a metal poor dominant stellar component, or it is related to a diffuse hot component, cannot be established with present data. New independent observational data sets, and accurate modelling, able to match all the observed properties of the two galaxies, are needed to better understand the physical characteristics of the unresolved stellar systems in both targets.

Nevertheless, the coupling of B -band with other optical or near- IR SBF measures, appears to be a promising method to unveil the properties of hot stellar components possibly hidden to other photometric indicators.

4.3. SBF colours and stellar populations properties in regions hosting type Ia Supernovae

The correlation between the SNe Ia peak magnitude and the host-galaxy morphology, i.e. the host stellar population, is well known since the work by Hamuy et al. (1996), showing that intrinsically fainter events occur in early-type galaxies, while luminous events are often seen in late-type galaxies. The results on the mean stellar population properties in the galaxies, discussed in the previous sections, seem to support the idea that old stellar system, i.e. old progenitors, are required for sub-luminous SNe Ia.

To better constrain the properties of the *local* stellar populations we have measured SBF and colours in the areas where the SNe Ia exploded, adopting a $25'' \times 25''$ square region. The results of the measurements are reported in Table 3, and shown with full triangles (for NGC 4621), and full squares (for NGC 4374) in the right panels of Figure 4.

First of all, we note that, from $B-V$, $V-R$ and $\bar{V}-\bar{R}$ data, the stellar population properties in the selected regions and in the main annulus (empty black symbols) appear remarkably homogeneous. Taking into account only such colours, we conclude that the stellar component in the regions hosting the three SNe Ia and the overall stellar population in the galaxies have quite similar properties, with all data matching SSP models of $[Fe/H] \gtrsim -0.4$ dex and $t \gtrsim 7$ Gyr. In any case, old ages are expected, supporting the results by Gallagher et al. (2008) based on spectroscopic data. It is interesting to note that the properties of the dominant stellar populations in the regions of the two SNe Ia host by NGC 4374 appear strikingly similar in these panels, nearly identical to each other, notwithstanding the large projected separation (~ 10 kpc) between the two regions.

Larger differences are seen between the three regions in the $B-\bar{V}$ versus $B-V$ panel (lower right panel in Figure 4). Due to the aforementioned stronger sensitivity of B -band SBF to changes of stellar population properties respect to other pass-bands, the larger scatter between the three SNe Ia is not surprising, and it might be possibly related to different levels of local “pollution” from a hot stellar component. Furthermore, the regions of NGC 4374 where SN 1991bg and SN 1957B exploded show a $\Delta\bar{B}-\bar{V} \sim 0.4$ mag, despite their nearly homogeneous $B-V$, $V-R$ and $\bar{V}-\bar{R}$ colours. Whether the $\Delta\bar{B}-\bar{V}$ is related to the SNe progenitors and their environment, and thus to the $\Delta B_{max} \sim 2.3$ mag between the two SNe Ia, or to problems with the P_r correction cannot be said using present data, and further analysis based on a richer sample is needed.

For what concerns NGC 4621, even including B -band SBF data we find a good matching between global and local, i.e. near SN 1939B, stellar population properties.

5. Conclusions

We have presented a detailed multi-band study of SBF magnitudes for two bright galaxies in the Virgo cluster, NGC 4621 and NGC 4374, based on deep B , V and R -band imaging data of the FORS2 camera at the VLT telescope.

Among the three bands available, the V and R have known empirical SBF calibrations useful to obtain the distances of the targets. Coupling our measurements with such calibrations, or with calibrations obtained from simple and composite stellar population models, we obtained accurate

distances for the two galaxies which agree very well with other distance estimates taken from literature. This demonstrates both the reliability of the measured SBF magnitudes and the goodness of the calibrations adopted. Taking advantage of the fact that various SBF distances, based on different calibrations for different filters, are available for the two targets, we have compared the average SBF distance moduli with other non-SBF ones, to check for any possible systematics. Although the sample of galaxies is statistically small, the results obtained seem to rule out the presence of possible bias on SBF distances.

Taking the median of all available SBF and non-SBF distance estimates, we estimated: $m - M = 30.98 \pm 0.17$ for NGC 4621, and $m - M = 31.22 \pm 0.16$ for NGC 4374.

The two target galaxies hosted a total of three SNIa events: one in NGC 4621, SN 1939B, and two in NGC 4374, SN 1957B and SN 1991bg, all classified as sub-luminous. Using some recent calibration relations based on decline rate and colours of the SN (Folatelli et al. 2010), and on the updated MLCS method (Jha et al. 2007) we find an excellent agreement between the SBF and SNeIa distances. A result that is very promising in view of a reduction of the number of “rungs” to bridge local to cosmological scale distances, i.e. to significantly reduce the systematic uncertainties on distances of objects at large distances and, consequently, on cosmological parameters.

We also carried out SBF measurements on *B*-band images, but such measures were rejected for distance analysis. The sensitivity of SBF magnitudes in this band to the stellar population properties makes unreliable any calibration in this band. We tentatively derived a *B*-band calibration based on SPoT models - which have proved being realistic in both *V* and *R* bands, as well as other studied bands (Biscardi et al. 2008) -, but the results obtained confirm that SBF magnitudes in such band are not well suited for any kind of distance analysis.

Thanks to the high quality of the data, we have succeeded in measuring SBF magnitudes in various galactic regions. Both integrated and SBF colours (excluding \bar{B}) seem to point out that the stellar population are relatively uniform along the galaxy radius. No sizable SBF gradient is observed in NGC 4374, while for NGC 4621 a small but non-negligible SBF gradient in *V* and *R* is observed, consistent with the known scheme of more metal poor dominant stellar populations at larger galactocentric radii (e.g. Cantiello et al. 2005). Given the fact that *i*) compared to *I*-band SBF *V* and *R* are more sensitive to stellar population properties (Blakeslee et al. 2001; Cantiello et al. 2003), and *ii*) \bar{I} gradients up to ~ 0.4 magnitudes were measured by Cantiello et al. (2005) on similar radial scales for a different set of targets, the negligible \bar{V} and \bar{R} gradients detected here might be explained by the position of the two objects within their host cluster. Since the two targets analysed are located in the regions with highest galaxy density in the Virgo cluster, in fact, this behaviour might be related to the major-merging events in such environment, which tend to smear out possible stellar population gradients (Kobayashi 2004).

Taking advantage of the multi-wavelength coverage of our data set, and of existing *I*, *z*, and *K*-band SBF measurements, we analysed the data of both galaxies in the SBF-colour versus integrated-colour and SBF-colour versus SBF-colour diagrams. This is the first SBF-analysis

carried out using SBF data in six different pass-bands. As a result we concluded that the dominant stellar component in the two galaxies is very similar, though NGC 4374 seems to be slightly more metal rich than NGC 4621.

If *B*-band measures are taken into account, the SBF colours of the two galaxies show non-negligible differences, with NGC 4621 having brighter SBF than NGC 4374. Given the known link between SBF magnitudes in blue bands and the properties of a hot old stellar component (Wortheley 1993a; Cantiello et al. 2003), we used the SPoT Stellar Population Synthesis code to simulate populations with “non-canonical” properties. In particular, to a solar metallicity old $t \sim 14$ Gyr population, we have 1) enhanced the content of hot HB stars (i.e., $\sim 50\%$ canonical HB and $\sim 50\%$ HHB), 2) added a very young (down to 30 Myr) diffuse secondary component, and 3) added a more metal poor SSP (down to $[Fe/H] \sim -2.3$ dex). Within the limits of the small number of data, and adopting as a razor the physical plausibility of the population mixing, the simulations seem to favour the HHB component scenario.

This is also supported by the fact that Brown et al. (2000) and Brown et al. (2008) find the presence of HHB stars in the compact elliptical galaxy M32 on the basis of *UV* observations. In this framework, it is relevant to recall that NGC 4621 is substantially brighter than NGC 4374 in the *UV* bands (Longo et al. 1991), and that the integrated properties of normal elliptical galaxies with bright *UV* emission are now interpreted as an effect of a diffuse hot stellar component (e.g. Park & Lee 1997). Thus, further analysis is required to better constrain the links between the *UV* emission and SBF in early type galaxies, also in view of the recent studies on the relation of *UV* with near-*IR* SBF amplitudes (Buzzoni & González-Lópezlira 2008), and larger samples of SBF colours in blue bands are required to provide further constraints to this scenario.

Finally, taking into account the integrated colours and \bar{V} plus \bar{R} SBF for the areas of the galaxies where type Ia Supernova exploded, we find no substantial differences between the local and the global stellar population properties in the galaxies. For SN 1939B and its host, NGC 4621, this is also true for *B*-band SBF data. On the contrary, there is a $\Delta\bar{B}-\bar{V} \sim 0.4$ mag difference between the regions of the two SNe host in NGC 4374, SN 1957B and SN 1991bg. Due to the quoted sensitivity of blue-band SBF to stellar population properties, such difference and, more in general, the scatter in $\bar{B}-\bar{V}$ between the three SNeIa might be related to different levels of local pollution from a hot stellar component, although for the case of SN 1991bg we cannot exclude the possible systematic effect of a low \bar{B} signal, comparable to the P_r correction.

In conclusion, the present set of SBF measures shows that optical to near-*IR* SBF magnitudes can be very effective to unveil the properties of global and/or local stellar populations in distant galaxies. In particular, if \bar{B} (or even SBF in bluer bands) are available, various constraints can be set to the role of hot field stars in normal ellipticals, at the same time multi-band SBF can be used to analyse the relation between SNe and local stellar population properties. Nevertheless, serious limitations are set by the small samples of measures still available, new observations are advisable to further study stellar population properties based on multi-colour SBF analysis.

Acknowledgements. M.C. acknowledges the support provided by the PRIN-INAF 2008 (PI. M. Marconi). We also thank the referee for

his very helpful suggestions. Based on data obtained from the ESO Science Archive Facility.

References

- Ajhar, E. A., Tonry, J. L., Blakeslee, J. P., Riess, A. G., & Schmidt, B. P. 2001, *ApJ*, 559, 584
- Barbon, R., Cappellaro, E., & Turatto, M. 1989, *A&AS*, 81, 421
- Bernardi, M., Renzini, A., da Costa, L. N., et al. 1998, *ApJ*, 508, L143
- Bertin, E. & Arnouts, S. 1996, *A&AS*, 117, 393
- Bertola, F. 1964, *AJ*, 69, 236
- Bertola, F., Capaccioli, M., Holm, A. V., & Oke, J. B. 1980, *ApJ*, 237, L65
- Biscardi, I., Raimondo, G., Cantiello, M., & Brocato, E. 2008, *ApJ*, 678, 168
- Blakeslee, J. P., Cantiello, M., Mei, S., et al. 2010, *ApJ*, 724, 657
- Blakeslee, J. P., Jordán, A., Mei, S., et al. 2009, *ApJ*, 694, 556
- Blakeslee, J. P., Vazdekis, A., & Ajhar, E. A. 2001, *MNRAS*, 320, 193
- Brocato, E., Capaccioli, M., & Condelli, M. 1998, *Memorie della Societa Astronomica Italiana*, 69, 155
- Brocato, E., Castellani, V., Poli, F. M., & Raimondo, G. 2000, *A&AS*, 146, 91
- Brocato, E., Matteucci, F., Mazzitelli, I., & Tornambe, A. 1990, *ApJ*, 349, 458
- Brown, T. M., Bowers, C. W., Kimble, R. A., Sweigart, A. V., & Ferguson, H. C. 2000, *ApJ*, 532, 308
- Brown, T. M., Smith, E., Ferguson, H. C., et al. 2008, *ApJ*, 682, 319
- Buzzoni, A. 1993, *A&A*, 275, 433
- Buzzoni, A. & González-Lópezlira, R. A. 2008, *ApJ*, 686, 1007
- Cantiello, M., Blakeslee, J., Raimondo, G., Brocato, E., & Capaccioli, M. 2007a, *ApJ*, 668, 130
- Cantiello, M., Blakeslee, J. P., Raimondo, G., et al. 2005, *ApJ*, 634, 239
- Cantiello, M., Raimondo, G., Blakeslee, J. P., Brocato, E., & Capaccioli, M. 2007b, *ApJ*, 662, 940
- Cantiello, M., Raimondo, G., Brocato, E., & Biscardi, I. 2009, *MemSAIt*, 80, 40
- Cantiello, M., Raimondo, G., Brocato, E., & Capaccioli, M. 2003, *AJ*, 125, 2783
- Code, A. D., Welch, G. A., & Page, T. L. 1972, in *NASA Special Publication*, Vol. 310, Scientific results from the orbiting astronomical observatory (OAO-2), ed. A. D. Code, 559
- Côté, P., Blakeslee, J. P., Ferrarese, L., et al. 2004, *ApJS*, 153, 223
- Folatelli, G., Phillips, M. M., Burns, C. R., et al. 2010, *AJ*, 139, 120
- Freedman, W. L., Madore, B. F., Gibson, B. K., et al. 2001, *ApJ*, 553, 47
- Gallagher, J. S., Garnavich, P. M., Berlind, P., et al. 2005, *ApJ*, 634, 210
- Gallagher, J. S., Garnavich, P. M., Caldwell, N., et al. 2008, *ApJ*, 685, 752
- González, R. A., Liu, M. C., & Bruzual A., G. 2004, *ApJ*, 611, 270
- Hamuy, M., Phillips, M. M., Suntzeff, N. B., et al. 1996, *AJ*, 112, 2391
- Han, Z. 2008, *A&A*, 484, L31
- Howell, D. A. 2001, *ApJ*, 554, L193
- Idiart, T. P., Michard, R., & de Freitas Pacheco, J. A. 2002, *A&A*, 383, 30
- Idiart, T. P., Silk, J., & de Freitas Pacheco, J. A. 2007, *MNRAS*, 381, 1711
- Jensen, J. B., Tonry, J. L., Barris, B. J., et al. 2003, *ApJ*, 583, 712
- Jensen, J. B., Tonry, J. L., & Luppino, G. A. 1998, *ApJ*, 505, 111
- Jensen, J. B., Tonry, J. L., Thompson, R. I., et al. 2001, *ApJ*, 550, 503
- Jerjen, H., Binggeli, B., & Barazza, F. D. 2004, *AJ*, 127, 771
- Jerjen, H., Freeman, K. C., & Binggeli, B. 1998, *AJ*, 116, 2873
- Jerjen, H., Freeman, K. C., & Binggeli, B. 2000, *AJ*, 119, 166
- Jha, S., Riess, A. G., & Kirshner, R. P. 2007, *ApJ*, 659, 122
- Jordán, A. 2004, *ApJ*, 613, L117
- Kaviraj, S., Sohn, S. T., O’Connell, R. W., et al. 2007, *MNRAS*, 377, 987
- Kobayashi, C. 2004, *MNRAS*, 347, 740
- Kosai, H., Kushida, R., Kato, T., Filippenko, A., & Newberg, H. 1991, *IAU Circ.*, 5400, 1
- Kuntschner, H., Lucey, J. R., Smith, R. J., Hudson, M. J., & Davies, R. L. 2001, *MNRAS*, 323, 615
- Landolt, A. U. 1992, *AJ*, 104, 340
- Lanoix, P. 1998, *A&A*, 331, 421
- Leibundgut, B., Tammann, G. A., Cadonau, R., & Cerrito, D. 1991, *A&AS*, 89, 537
- Longo, G., Ceriello, A., & Capaccioli, M. 1991, *A&AS*, 90, 375
- Mei, S., Blakeslee, J. P., Côté, P., et al. 2007, *ApJ*, 655, 144
- Minkowski, R. 1964, *ARA&A*, 2, 247
- Pahre, M. A. & Mould, J. R. 1994, *ApJ*, 433, 567
- Park, J. & Lee, Y. 1997, *ApJ*, 476, 28
- Phillips, M. M., Lira, P., Suntzeff, N. B., et al. 1999, *AJ*, 118, 1766
- Press, W. H., Teukolsky, S. A., Vetterling, W. T., & Flannery, B. P. 1992, *Numerical recipes in FORTRAN. The art of scientific computing* (Cambridge: University Press, —c1992, 2nd ed.)
- Raimondo, G. 2009, *ApJ*, 700, 1247
- Raimondo, G., Brocato, E., Cantiello, M., & Capaccioli, M. 2005, *AJ*, 130, 2625
- Raimondo et al. 2011, in preparation
- Riess, A. G., Filippenko, A. V., Challis, P., et al. 1998, *AJ*, 116, 1009
- Schlegel, D. J., Finkbeiner, D. P., & Davis, M. 1998, *ApJ*, 500, 525
- Scott, N., Cappellari, M., Davies, R. L., et al. 2009, *MNRAS*, 398, 1835
- Sersic, J. L. 1968, *Atlas de galaxias australes* (Cordoba, Argentina: Observatorio Astronomico, 1968)
- Shoppell, P. L., Bland-Hawthorn, J., & Malin, D. F. 1993, *AJ*, 106, 1344
- Sirianni, M., Jee, M. J., Benítez, N., et al. 2005, *PASP*, 117, 1049
- Sodemann, M. & Thomsen, B. 1996, *AJ*, 111, 208
- Tonry, J. & Schneider, D. P. 1988, *AJ*, 96, 807
- Tonry, J. L., Ajhar, E. A., & Luppino, G. A. 1990, *AJ*, 100, 1416
- Tonry, J. L., Blakeslee, J. P., Ajhar, E. A., & Dressler, A. 2000, *ApJ*, 530, 625
- Tonry, J. L., Dressler, A., Blakeslee, J. P., et al. 2001, *ApJ*, 546, 681
- Turatto, M., Benetti, S., Cappellaro, E., et al. 1996, *MNRAS*, 283, 1
- Wang, X., Wang, L., Pain, R., Zhou, X., & Li, Z. 2006, *ApJ*, 645, 488
- Worthey, G. 1993a, *ApJ*, 415, L91+
- Worthey, G. 1993b, *ApJ*, 409, 530
- Worthey, G. 1994, *ApJS*, 95, 107
- Zwicky, F. 1942, *ApJ*, 96, 28